Research Article BEU Fen Bilimleri Dergisi 15(2): 750-766 (2026) DOI: 10.17798/bitlisfen.1834019

BİTLİS EREN UNIVERSITY
FEN BİLİMLERİ DERGİSİ
ISSN: 2147-3129 / e-ISSN: 2147-3188

INVESTIGATION OF THE EFFECT OF EARTHQUAKE CHARACTERISTICS, SOIL PROPERTIES AND DAMPING ON THE INPUT ENERGY OF STRUCTURES

Yusuf TURGUT [1], **Serkan ENGİN** [2*] Hasan SESLİ [1]

[1] *Yalova University, Civil Engineering Department, Yalova, Türkiye*
[2] *Kocaeli University, Civil Engineering Department, Kocaeli, Türkiye*
*** Corresponding Author:** serkan.engin@kocaeli.edu.tr

Article Info

Received: *December 1, 2025*
Revised: *April 2, 2026*
Accepted: *April 9, 2026*

Keywords
Energy-Based Design,
Input Energy,
Single Degree of Freedom System,
Damping Ratio,
Soil Class,
Forward Directivity Effect.

ABSTRACT

This study investigates the combined influence of forward directivity (FD), site class, and damping ratio on the seismic input energy demand of linear single-degree-of-freedom (SDOF) systems using an energy-balance framework. Four near-fault ground-motion sets with FD and non-forward directivity (NFD) were compiled for ZC and ZD soil classes, and elastic input energy spectra were computed for damping ratios of 2%, 5%, and 20%. Analysis of the earthquake records showed that increasing the damping ratio from 2% to 20% reduced the peak average input energy by approximately 35-40% for the selected records. The effect of forward directivity in the selected ground motion is that the average input energy increases by approximately 35-50% in the ZC soil class, while this increase is almost three times greater in the ZD soil class. Overall, increasing damping systematically reduces peak mean input energy, while FD effects markedly amplify energy demand, especially on soft soils. These findings underline that near-fault pulse-like characteristics and site conditions should be jointly considered when interpreting energy-based seismic demand.

1. INTRODUCTION

Force-based design and displacement-based design are generally used in the seismic design of structures. Many codes provide requirements based on these design principles, such as the Design of Structures for Earthquake Resistance (Eurocode 8), the Federal Emergency Management Agency (FEMA 440), and the Turkish Building Earthquake Code (TBEC, 2018) [1-3]. In force-based design, the loads on each section are determined by analyzing the structure under predicted loads, and the resulting loads are compared with each section's load capacity. In the displacement-based design approach, first recommended by Kowalsky et al. (1994), the expected deformation of the structural section under external loads is compared with its deformation capacity [4].

Nowadays, it is accepted that the best way to represent the impact of an earthquake is by the amount of energy it generates [5]. Therefore, methods based on energy dissipation in a structure are considered a better design approach, and the energy-based design approach is presented as an alternative to traditional methods [6-9]. In this approach, design is achieved by balancing the structure's capacity to dissipate earthquake energy with the energy released by the earthquake [10]. Although not currently included in design codes, the energy-based design approach provides an analysis by expressing earthquake effects in terms of their energy components. There are various academic approaches to the energy-based design approach, first proposed by Housner in 1956, that can also be used in building design as we approach the present day [11]. Input energy, a critical parameter within energy-based design, is an important indicator of the structure's seismic performance because it represents the total energy input into the system. Input energy represents the total amount of energy to which a structural system is exposed under the influence of an earthquake and equals the sum of kinetic energy, damping energy, elastic energy, and hysteretic energy in the system [12-14]. Many studies have examined the determination of input energy

License: CC BY-NC 4.0

and factors affecting it. In studies on the determination of input energy, Goel (1997) analyzed the distribution of energy input using energy balance equations for a single-degree-of-freedom system [15]. In addition to this study, Benavent-Climent et al. (2004) examined input energy in more detail by separating the energy equations into kinetic energy, damping energy, elastic energy, and hysteretic energy [14]. Since input energy results from the interaction between ground motion and the structure, the properties of the structure are as important as those of the ground motion. Hosseini and Vaseghinia (2008) stated in their study that treating the input energy solely as the energy generated by earthquake motion would be inadequate and that the structure's properties also affect the input energy [16]. Therefore, the structure's behavior significantly affects the distribution and dissipation of incoming energy. Since the nonlinear behavior of the structure allows for greater energy dissipation in the cross-sections, the energy-based approach is particularly important for structures exhibiting nonlinear behavior [17]. Dindar et al. (2015) aimed to calculate a more comprehensive energy input by accounting for differences in soil classes and earthquake characteristics [18]. Yalçın et al. (2021) proposed a novel energy-based design approach to directly determine both the seismic demand and energy dissipation capacities of reinforced concrete (RC) frame elements through their inelastic behavior and determined that the element and overall performance targets of the proposed approach are comparable to those of the displacement approach [19].

Vibrations induced by external forces, such as earthquake loads, are reduced by damping. A large portion of the resulting input energy is dissipated by damping [20,21]. Increasing the damping ratio used in structures is expected to increase the energy absorbed by the structures. A study of a single-degree-of-freedom system using different damping ratios under near-source earthquake records showed that damping ratios have a significant effect on energy factors [12]. Increasing the damping ratio from 2% to 10% reduces input energy by approximately 50% [22]. Since most earthquake codes assume a 5% damping ratio for conventional structures, earthquake spectra are generated accordingly. However, for some structures, the damping ratio may differ from the standard 5% [23]. For example, the number of stories in buildings is also increasing in parallel with the increasing global population and urbanization. The damping ratio in such high-rise buildings is lower than in standard structures [24]. Furthermore, the damping ratio in structures equipped with seismic isolators and dampers can exceed the standard ratio [25]. Therefore, treating the damping ratio as a variable enables a more accurate assessment of structures' earthquake energy absorption capacity.

Building performance is affected not only by the materials and structural systems constituting the building, but also by the soil class on which the structure is located. Numerous studies have shown that the energy input to the system varies with soil class [12,20,26-31]. Okur and Erberik (2012 and 2014) reported that the energy input will be greater in soft soils [27,28]. Sucuoğlu and Alıcı (2019) investigated the effect of energy dissipation requirements on systems under the influence of near-fault earthquakes across different soil classes, using a model they developed to input energy. Their study revealed that ground motions in soft soils demand significantly more energy than those in hard soils [29]. Another study compared input energy in single-degree-of-freedom systems and found that the increase in total input energy was directly related to soil weakening [12]. In the study by Hasanoğlu et al. (2024), it was shown that considering the input energy along with spectral acceleration for the selection and scaling of earthquake records can significantly reduce the deviation in structural response, especially for structures located on hard soils [31]. In this context, the energy transferred to a structure during an earthquake can vary depending on soil conditions. Therefore, the influence of soil is considered in the design phase of a structure.

According to the definition of Somerville et al. (1997), ground motion within 20 km of the fault is called near-field ground motion, and it is accepted that these records transfer more energy to the structure [32]. Studies conducted in subsequent years also determined that near-source ground motions release greater energy [30,33]. It is widely accepted that near-field earthquake records impart more energy to structures. However, structures located in the near field and in the direction of the fault rupture are exposed to more energy than those in the opposite direction. These ground motions, referred to as forward-directivity effects, are earthquake records that transfer energy instantaneously, producing high velocities and large displacements. These ground motions, which contain large-amplitude impulses, transfer energy to the structure with high acceleration over a short duration. During propagation of non-forward directivity,

ground motions located opposite the rupture direction do not exhibit dominant pulse-like motions, and energy is transferred to the structures over a longer period. In addition to the presence of forward directivity, the interaction between the structural natural period and the pulse characteristics of near-fault ground motions plays a key role in determining seismic energy demand. Previous studies have shown that when the pulse period of forward-directivity ground motions approaches the fundamental period of the structure, a resonance-like effect may occur, resulting in significantly increased velocity, displacement, and energy demands [33,34]. Baker (2007) demonstrated that pulse-like ground motions with pulse periods comparable to the structural period can concentrate a large portion of the input energy into a short time interval, leading to amplified seismic demands. Therefore, the seismic input energy demand of structures subjected to forward-directivity effects is governed not only by soil conditions and damping ratio but also by the compatibility between the pulse period of the ground motion and the structure's dynamic characteristics [34]. The study by Bigdeli et al. (2008) shows the acceleration, velocity, and displacement-time graphs of different near-field records of the Chi-Chi earthquake, with and without forward directivity effects, in Figure 1 [35]. Figure 1(a) shows that the change in acceleration time of ground motion with forward directivity exhibits abrupt variations compared with ground motion without forward directivity shown in Figure 1(b).

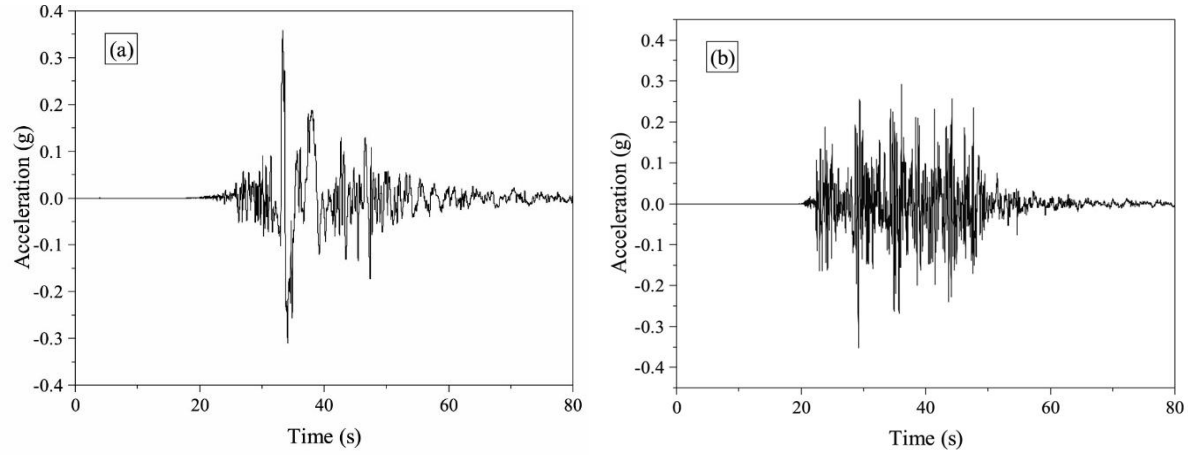


*Figure 1. Acceleration-time graphs of the Chi-Chi earthquake (*a*) earthquake record with forward directivity (FD) effect (TCU036); (b) earthquake record with non-forward directivity (NFD) effect (TCU089). [35]*

While some studies report that increased damping may significantly reduce input energy by dissipating a larger portion of seismic demand [36], others suggest that input energy is primarily governed by ground motion characteristics and is only weakly dependent on damping [11]. A similar evolution is observed in the terminology used for near-fault ground motions. Although the concept of 'near-fault' motion was widely introduced in the late 1990s [32] recent literature increasingly adopts the classification of pulse-like, and non-pulse-like ground motions based on velocity pulse characteristics rather than fault proximity alone [36]. In this study, forward-directivity records are therefore interpreted within this broader pulse-like framework, and the results are discussed in light of these ongoing debates.

Forward directivity (FD) refers to the enhancement of ground-motion intensity at sites located in the direction of fault rupture propagation, caused by the constructive interference of radiated seismic waves as the rupture front advances toward the site. A hallmark of FD motions is the presence of a large, coherent pulse in the velocity time history (often termed 'pulse-like' motion), -which concentrates a substantial portion of seismic energy within a short time window and can increase displacement- and energy-related demands. In contrast, non-forward directivity (NFD) motions are typically recorded at locations that are not aligned with the rupture propagation direction (including backward directivity cases), and they do not exhibit a dominant long-period velocity pulse; instead, energy is delivered more gradually throughout the record.

The observed differences between forward directivity (FD) and non-forward directivity (NFD) ground motions and between different soil classes can be interpreted in terms of seismic energy flux and

impedance. Seismic impedance, defined by the product of soil density and shear-wave velocity, controls the transmission and reflection of seismic energy at the soil–structure interface. Previous studies by Şafak (2001) have shown that softer soils with lower impedance facilitate more efficient transmission of long-period and pulse-like seismic energy, whereas stiffer soils tend to reflect a larger portion of the incoming energy. Under near-fault FD conditions, the concentration of energy into velocity pulses further increases the energy flux entering the structure, providing a physical explanation for the higher input energy demand observed on ZD soils compared to ZC soils in this study [37].

Although energy balance is more critical for nonlinear structures, this study examined linear structural behavior to observe the effects of different soil conditions and damping ratios. To determine the average input energy required by earthquakes, four earthquake sets were created from ground motion records for the ZC and ZD soil classes, with and without a forward directivity effect. Input energy spectra for the earthquakes in these record sets were computed for damping ratios of 2%, 5%, and 20%. The results were compared to examine the effects of forward directivity, soil type, and damping ratio on average input energy.

2. MATERIAL AND METHOD

Although the concept of energy balance was first introduced by Housner in 1956, the concept of energy balance in structures was defined by Chopra in 1995 as in Equation (2) using the equation of motion of the single degree of freedom system given in Equation (1) [11,38].

$$m\ddot{u} + c\dot{u} + f_s(u) = -m\ddot{u}_g(t) \tag{1}$$

In Equation (1), m represents the mass, $\ddot{u}$ represents the acceleration, c represents the damping coefficient, and $\dot{u}$ represents the velocity. Furthermore, f_s in the equation represents the resistive force, and u represents the relative displacement relative to the ground. $\ddot{u}_g(t)$ on the right-hand side of the equation, represents the ground acceleration. The energy parameters can be expressed by integrating Equation (1) over the relative displacement.

$$\int_0^{u(t)} m\ddot{u}\,du + \int_0^{u(t)} c\dot{u}\,du + \int_0^{u(t)} f_s(u)\,du = -\int_0^{u(t)} m\ddot{u}_g(t)du \tag{2}$$

Equation (2) is the energy balance equation of the single-degree-of-freedom system. This equation can be expressed, as given in Equation (3), as a function of time by taking into account the expression $\dot{u}du=d$.

$$\underbrace{\int_0^t m\ddot{u}\dot{u}dt}_{E_K} + \underbrace{\int_0^t c\dot{u}^2dt}_{E_D} + \underbrace{\int_0^t f_s(u)\dot{u}dt}_{E_E+E_H} = \underbrace{-\int_0^t m\ddot{u}_g(t)\dot{u}dt}_{E_I} \tag{3}$$

The first term on the left-hand side of Equation 3 represents the kinetic energy of the structure (E_K), the second term represents the damping energy (E_D), and the third term represents the sum of the elastic strain energy (E_E) and the hysteretic energy (E_H). The remaining part of the equation on the right-hand side represents the total input energy (E_I) of the structure. Accordingly, Equation (3) can be written as follows.

$$E_K + E_D + E_E + E_H = E_I \tag{4}$$

Since E_H, which shows the hysteretic energy in Equation (4), does not exist in elastic systems ($E_H = 0$), the general equation to be used for elastic systems can be written as in Equation (5).

$$E_K + E_D + E_E = E_I \tag{5}$$

The damping ratio is a parameter that indicates how much of the system's total input energy is dissipated through damping. Different damping ratios (ξ) are used to examine the effect of damping energy, expressed in Equation (5), on structures. In this study, the damping ratios (ξ) for the single-degree-of-freedom system are taken as 2%, 5%, and 20%. Using Equation (5), the input energies demanded by earthquakes and the average input energies of selected earthquake records were obtained using Excel VBA Macro and MATLAB R2024b software [39].

In this study, a linear single degree of freedom (SDOF) system, shown in Figure 2, represents the structure's fundamental vibration mode. The system consists of a lumped mass, linear elastic stiffness, and viscous damping and is characterized by a fixed fundamental period T = 1.0 s and damping ratios of 2%, 5%, and 20%. This simplified representation allows direct investigation of the influence of ground motion characteristics, soil class, and damping ratio on seismic input energy, without the additional complexity introduced by higher-mode effects.

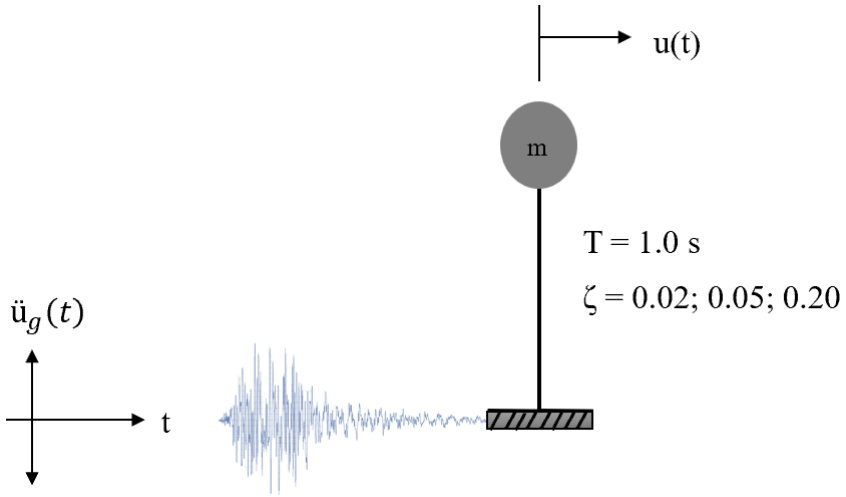


Figure 2. The SDOF system used in the study.

3. SELECTED EARTHQUAKE RECORDS

This study examines 11 earthquake sets from ZC and ZD soil classes, each analyzed both with and without forward directivity effects, to calculate input energy for various ground motions and conditions. To carry out this analysis, forty-four ground motion records were selected from the Pacific Earthquake Engineering Research Center (PEER) NGA West 2 database [40]. These records cover earthquake magnitudes ranging from 6.0 to 8.0 Mw. Additionally, to maintain dataset diversity, a maximum of 3 records were selected for each earthquake.

Table 1. Forward directivity (FD) earthquake records from the ZC soil class.

RSN	Earthquake	Station	Year	M_w	V_{S30} (m/s)	Soil Class	R_{JB} (km)	PGA (g)	PGV (cm/s)	PGD (cm)
292	Irpinia	Sturno	1980	6.90	382.00	ZC	6.78	0.28	52.80	21.96
451	Morgan Hill	Coyote Lake Dam	1984	6.19	561.43	ZC	0.53	0.94	67.40	13.48
3746	Cape Mendocino	Centerville Beach	1992	7.01	459.04	ZC	16.44	0.45	50.40	14.02
1086	Northridge-01	Olive View	1994	6.69	440.54	ZC	1.74	1.74	94.53	24.16
1510	Chi-Chi	TCU075	1999	7.62	573.02	ZC	0.89	0.30	79.04	70.59
1511	Chi-Chi	TCU076	1999	7.62	614.98	ZC	2.74	0.40	56.02	38.62
1529	Chi-Chi	TCU102	1999	7.62	714.27	ZC	1.49	0.27	80.10	75.33
4040	Bam	Bam	2003	6.60	487.40	ZC	0.05	0.74	88.28	27.18
4097	Parkfield-02	Slack Canyon	2004	6.00	648.09	ZC	1.60	0.31	39.47	7.50
4211	Niigata	NIG021	2004	6.63	418.50	ZC	10.21	1.48	51.76	10.66
4847	Chuetsu-oki	Joetsu Kakizakiku	2007	6.80	383.43	ZC	9.43	0.42	70.08	25.15

Table 1 presents forward-directivity earthquakes in the ZC class. The first column of the table shows the record number (RSN) of the selected earthquake in the PEER database. The second column shows the earthquake from which the record was taken.

The third column shows the recording station. The year of the earthquake, the earthquake moment magnitude (M_w), the ground shear wave velocity (V_{S30}), the ground class, the distance between the earthquake location and the fault (R_{JB}), the maximum ground acceleration (PGA), maximum ground velocity (PGV), and maximum displacement (PGD) in the record are given.

For the records in Table 1, the V_{S30} values range from 382.00 m/s to 714.27 m/s, and these records are classified as the ZC soil class according to the TBEC soil classification. For the selected records, R_{JB} values vary between 0.05 km and 16.44 km, PGA values between 0.27 g and 1.48 g, PGV values between 39.47 cm/s and 94.53 cm/s, and PGD values between 7.50 cm and 75.33 cm.

Table 2 presents records of earthquake sets selected from the ZC class. These records do not include forward directivity effects. V_{S30} values in Table 2 range from 382.12 m/s to 760.00 m/s. They are classified in the ZC soil group according to the TBEC soil classification. The R_{JB} distances between the records range from 0.11 km to 14.82 km. PGA values range from 0.44 g to 1.16 g, PGV values range from 21.34 cm/s to 69.07 cm/s, and PGD values range from 1.87 cm to 23.99 cm.

Table 2. Non-forward directivity (NFD) earthquake records from the ZC soil class.

RSN	Earthquake	Station	Year	M_w	V_{S30} (m/s)	Soil Class	R_{JB} (km)	PGA (g)	PGV (cm/s)	PGD (cm)
230	Mammoth Lakes	Convict Creek	1980	6.06	382.12	ZC	1.10	0.44	23.80	5.16
495	Nahanni	Site 1	1985	6.76	605.04	ZC	2.48	1.16	40.41	8.43
753	Loma Prieta	Corralitos	1989	6.93	462.24	ZC	0.16	0.50	48.34	11.39
1111	Kobe	Nishi-Akashi	1995	6.90	609.00	ZC	7.08	0.47	39.47	11.85
1197	Chi-Chi	CHY028	1999	7.62	542.61	ZC	3.12	0.77	69.07	23.99
1201	Chi-Chi	CHY034	1999	7.62	378.75	ZC	14.82	0.30	42.13	14.73
8165	Düzce	IRIGM496	1999	7.14	760.00	ZC	4.21	1.00	40.04	17.09
3964	Tottori	TTR007	2000	6.61	469.79	ZC	11.28	0.74	37.09	15.07
4114	Parkfield-02	Fault Zone 11	2004	6.00	541.73	ZC	3.12	0.83	21.34	1.87
2419	Niigata	NIGH01	2004	6.63	480.40	ZC	0.49	0.74	61.31	14.53
8158	Christchurch	LPCC	2011	6.20	649.67	ZC	2.52	0.93	40.64	13.53

Table 3 presents ground motions with forward directivity effects for the ZD soil class. V_{S30} values for these records range from 198.00 m/s to 348.69 m/s and are classified as ZD soil group according to TBEC. For the selected ground motions, R_{JB} ranges from 0.18 km to 9.94 km, PGA from 0.32 g to 0.78 g, PGV from 65.20 cm/s to 117.10 cm/s, and PGD from 12.62 cm to 81.78 cm.

Table 3. Forward directivity (FD) earthquake records from the ZD soil class.

RSN	Earthquake	Station	Year	M_w	V_{S30} (m/s)	Soil Class	R_{JB} (km)	PGA (g)	PGV (cm/s)	PGD (cm)
180	Imperial Valley	El Centro Array#5	1979	6.53	205.63	ZD	1.76	0.41	78.29	62.49
723	Superstation Hill	Parachute TestSite	1987	6.54	348.69	ZD	0.95	0.43	102.20	34.98
1044	Northridge-01	Fire Station	1994	6.69	269.14	ZD	3.16	0.65	86.68	25.79
1054	Northridge-01	Pardee-SCE	1994	6.69	325.67	ZD	5.54	0.42	65.20	12.62
1106	Kobe	KJMA	1995	6.90	312.00	ZD	0.94	0.78	83.57	19.74
1114	Kobe	Port Island	1995	6.90	198.00	ZD	3.31	0.32	73.10	35.27
1244	Chi-Chi	CHY101	1999	7.62	258.89	ZD	9.94	0.38	91.28	60.73
1503	Chi-Chi	TCU065	1999	7.62	305.85	ZD	0.57	0.69	114.17	81.78
2114	Denali	TAPS	2002	7.90	329.40	ZD	0.18	0.32	94.23	45.89
6906	Darfield	GDLC	2010	7.00	344.02	ZD	1.22	0.73	117.10	77.59
6911	Darfield	HORC	2010	7.00	326.01	ZD	7.29	0.47	77.77	48.27

Table 4 presents ground motion records from Class ZD, excluding any forward directivity effects. The V_{S30} for these records ranges from 191.06 to 355.18 m/s, which corresponds to class ZD soils as defined by TBEC. Among the examined records, R_{JB} distances range from 3.92 km to 19.74 km; PGA values

range from 0.18 g to 0.70 g; PGV values range from 23.55 cm/s to 64.77 cm/s; and PGD values range from 3.73 cm to 42.72 cm.

Table 4. Non-forward directivity (NFD) earthquake records from the ZD soil class.

RSN	Earthquake	Station	Year	M_w	V_{S30} (m/s)	Soil Class	R_{JB} (km)	PGA (g)	PGV (cm/s)	PGD (cm)
30	Parkfield	Cholame	1966	6.19	289.56	ZD	9.58	0.38	23.55	5.42
126	Gazli	Karakyr	1976	6.80	259.59	ZD	3.92	0.70	64.77	24.08
174	Imperial Valley	ElCentroArray#11	1979	6.53	196.25	ZD	12.56	0.38	40.77	21.52
848	Landers	Coolwater	1992	7.28	352.98	ZD	19.74	0.35	33.22	16.83
3749	CapeMendocino	Fortuna Fire	1992	7.01	355.18	ZD	16.54	0.31	34.31	18.15
1049	Northridge-01	Pacific Palisades	1994	6.69	191.06	ZD	13.34	0.34	23.71	3.73
1101	Kobe	Amagasaki	1995	6.90	256.00	ZD	11.34	0.31	45.04	27.43
1158	Kocaeli	Duzce	1999	7.51	281.86	ZD	13.60	0.32	56.11	31.87
1536	Chi-Chi	TCU110	1999	7.62	212.72	ZD	11.58	0.18	52.00	31.22
5991	El Mayor	ElCentroArray#10	2010	7.20	202.85	ZD	19.36	0.37	49.96	31.54
5992	El Mayor	ElCentroArray#11	2010	7.20	196.25	ZD	15.36	0.50	59.80	42.72

Figure 3(a) shows the moment magnitudes of the earthquakes from which the acceleration records used in the study were taken. The records of earthquakes with moment magnitudes between 6.0 and 8.0 are uniformly distributed.

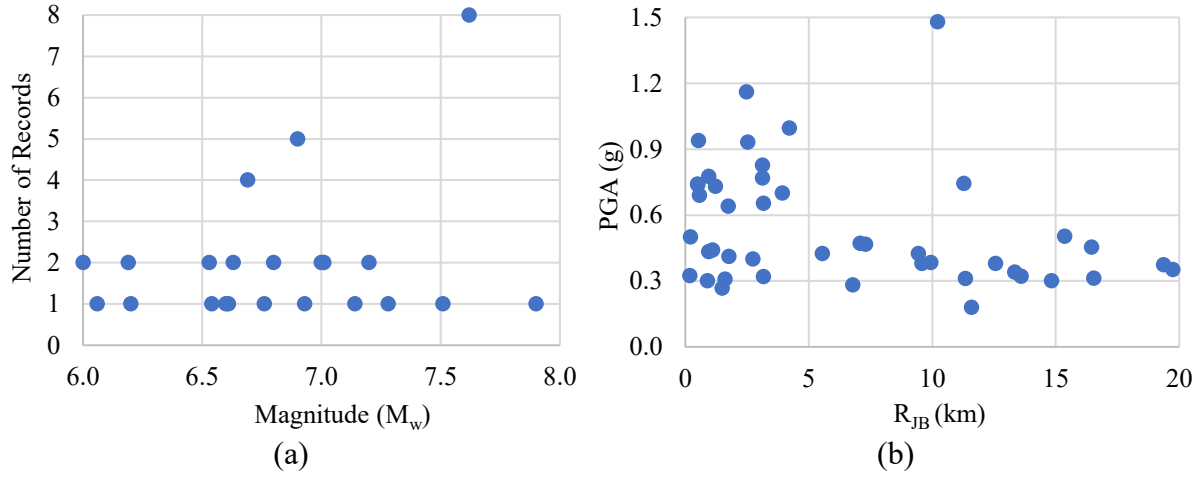


Figure 3. Characteristics of the selected earthquake records (a) earthquake magnitude and the number of records selected from these earthquakes; (b) distribution of the selected earthquake records according to R_{JB} (km) and PGA (g) values.

Figure 3(b) presents the PGA distributions of the ground motions used in the study by their R_{JB} distances. The Joyner-Boore distances range from 0 to 20 km, with PGA values from 0.18 g to 1.48 g. Most selected ground motions have PGA values concentrated between 0.3 g and 0.8 g, as shown in Figure 3(b).

Figure 4 shows variations in spectral acceleration periods and their averages for selected earthquake records. Figure 4 shows the spectral acceleration variations of the records for the following groups: (a) ZC&FD, (b) ZC&NFD, (c) ZD&NFD, and (d) ZD&NFD. Figure 5 compares the average spectral acceleration graphs among these groups. Although these graphs diverge slightly in the short-period region, they are similar in the long-period region.

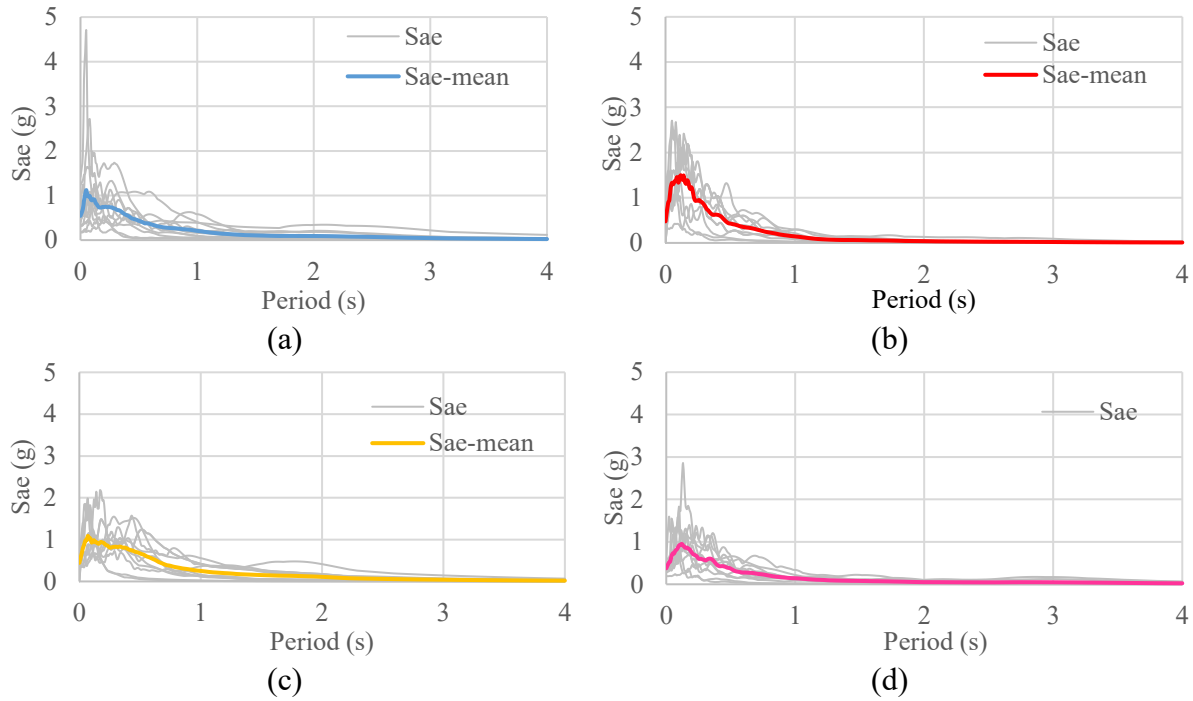


Figure 4. Spectral acceleration-period plots for selected earthquake records (a) for ZC&FD; (b) for ZC&NFD; (c) for ZD&FD; (d) for ZD&NFD.

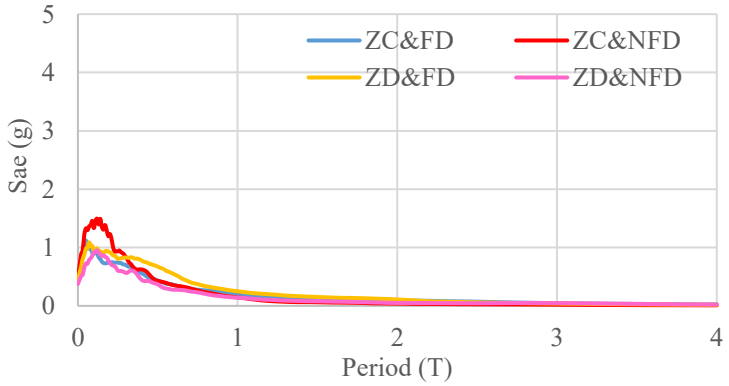


Figure 5. Comparison of mean spectral acceleration graphs for selected records.

Since each earthquake has unique characteristics, forward-directivity and non-forward-directivity ground motions for soil classes ZC and ZD are listed in Tables 1 and 4, respectively. The SeismoSelect 2025 [41] program was used to determine the components of characteristic values, such as R_{JB}, V_{S30}, PGA, and PGV, for the 44 selected earthquake records. When the generated tables are examined together, the 2004 Niigata earthquake (magnitude 6.63 Mw; record number 4211), measured at station NIG021, has the highest PGA value. The PGA of this ground motion is 1.48 g. On the other hand, the earthquake with the highest PGV was the 2010 Darfield earthquake (record number 6906), recorded at station GLDC. This value is 117.10 cm/s. Finally, the highest PGD was recorded at seismic station TCU065 (RSN 1505) during the 1999 Chi-Chi earthquake, measuring 81.78 cm.

4. OBTAINED DATA

A software program was created using Equation (5) in MATLAB R2024b [39] and an Excel VBA macro. This program generated the input energy spectrum for each earthquake. In the analysis, the total energy entering the system equals the sum of the kinetic, elastic strain, and damping energies, as shown in Equation (3).

Figure 6 shows, for example, the input energy-time graph obtained from the Chi-Chi earthquake, number 1529 RSN, shown in Table 1, according to equation (3). The blue curves in the graph represent elastic strain energy; the red curve represents kinetic energy; and the green curve represents damping energy. The black curve, which represents the sum of these energies, indicates the change in total input energy over the duration of the ground motion. As shown in the graph, a large portion of the total energy is due to damping.

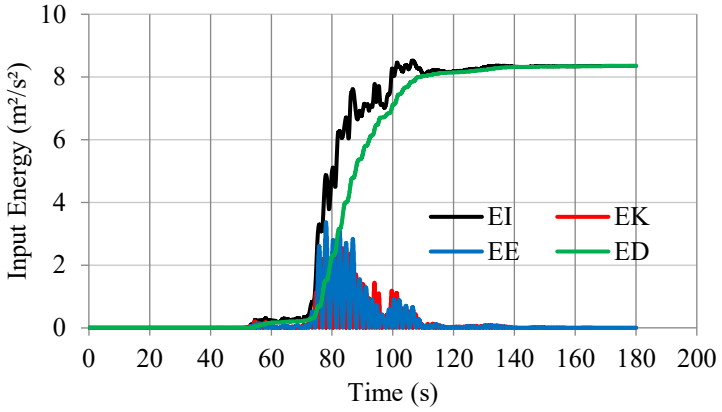


Figure 6. Forward directivity earthquake load from ZC soil class.

Using this approach, the input energies for all ground motions in the record sets listed in Tables 1-4 were calculated and then averaged to obtain the mean input energy for each record set. Furthermore, to assess the damping effect, the analyses used the average input energies corresponding to damping ratios of 2%, 5%, and 20%. The following sections compare the average input energy values at these three damping ratios for each earthquake set studied.

Figure 7 shows the input energy E_I generated by ground motions containing FD for the ZC soil class under different damping ratios. The input energy for the earthquake record, obtained using Equation (5) and plotted in black in Figure 6, is shown for the entire record set in Figure 7. The input energy of the 11 ground motions in the record set is plotted in light colors, and the average of the data set is shown in dark colors. Figure 7(a) shows the input energy of ground motions under a 2% damping ratio; Figure 7(b) shows the input energy of ground motions under a 5% damping ratio; and Figure 7(c) shows the input energy of ground motions under a 20% damping ratio and their average.

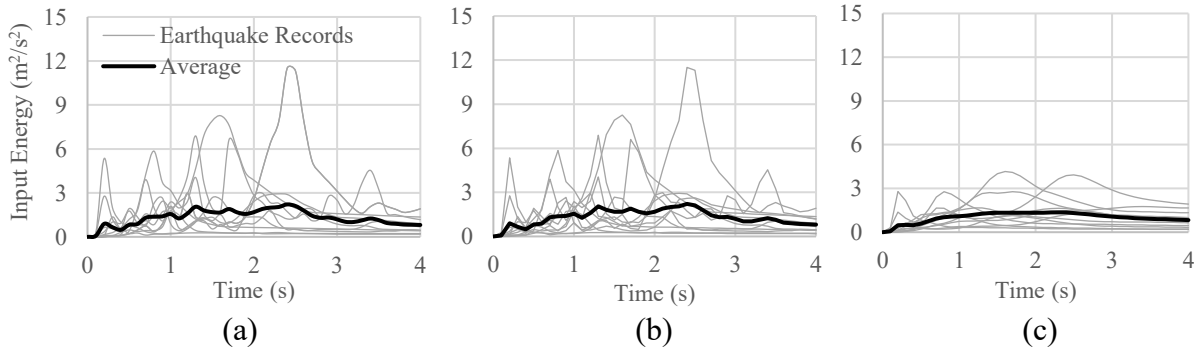


Figure 7. Earthquakes including forward directivity (FD) effect in ZC soil class data set and their average (a) under 2% damping ratio; (b) under 5% damping ratio; (c) under 20% damping ratio.

Figure 8 shows the input energy generated by NFD ground motions for the ZC soil class and the average of these values under different damping ratios. E_I The value obtained using Equation (5) is plotted for the entire record set in Figure 8. The input energies of the ground motions in Table 2 are shown in light colors. Figure 8(a) shows the input energies of ground motions at a 2% damping ratio. Figure 8(b) shows the input energies of the ground motions at a 5% damping ratio. Figure 8(c) shows the input energies of ground motions at a 20% damping ratio and their averages.

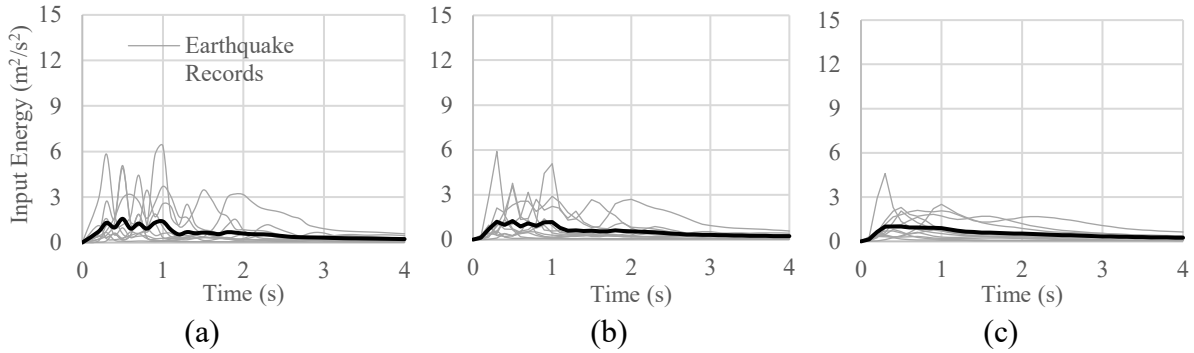


Figure 8. Earthquakes which have non-forward directivity (NFD) effect in ZC soil class data set and their average (a) under 2% damping ratio; (b) under 5% damping ratio; (c) under 20% damping ratio.

Figure 9 presents the input energies, generated by earthquake records containing FD, for the ZD site class at different damping ratios. The input energy for each ground motion is calculated using Equation (5) and plotted in light colors. The average input energy for the records in Table 3 is shown using dark colors for each damping ratio. Figures 9(a), 9(b), and 9(c) display input energies for 2%, 5%, and 20% damping ratios, respectively, along with their averages.

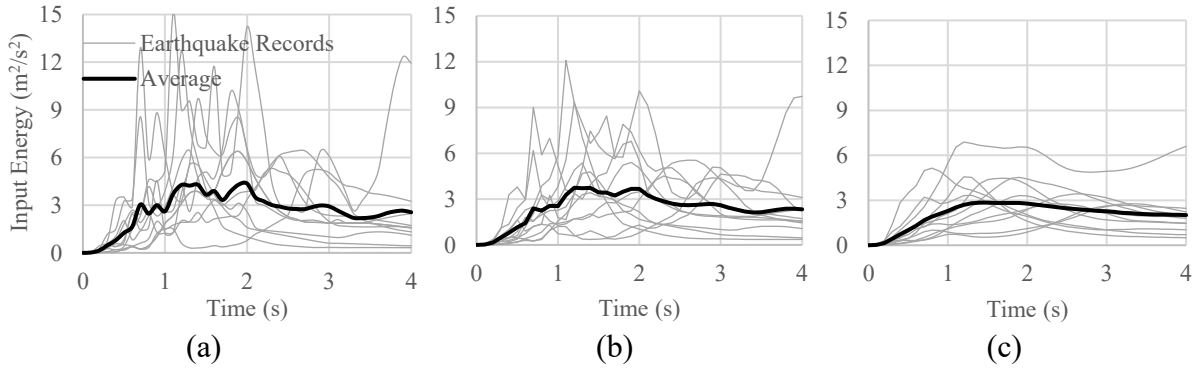


Figure 9. Earthquakes including forward directivity (FD) effect in ZD soil class data set and their average (a) under 2% damping ratio; (b) under 5% damping ratio; (c) under 20% damping ratio.

Figure 10 shows the input energy generated by NFD ground motions for the ZD soil class across different damping ratios. The input energy for a single earthquake record, drawn in black in Figure 3, is plotted across the entire record set in Figure 10.

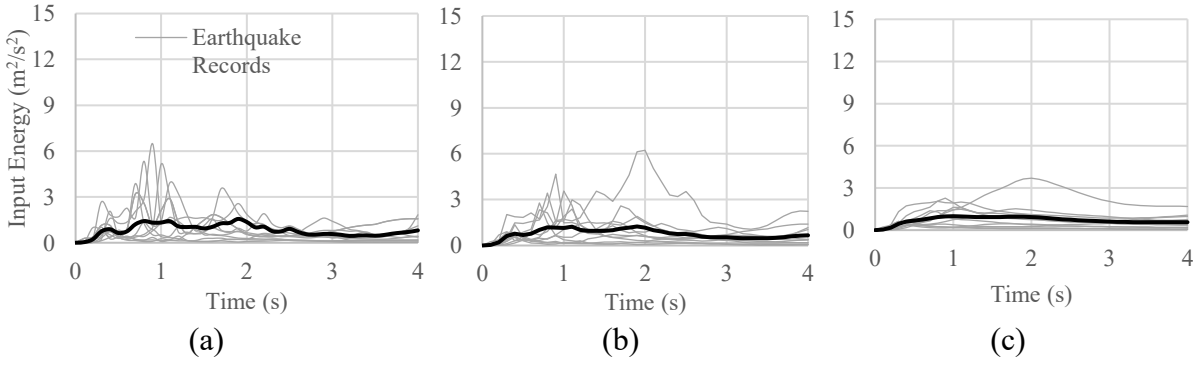


Figure 10. Earthquakes which have non-forward directivity (NFD) effect in ZD soil class data set and their average (a) under 2% damping ratio; (b) under 5% damping ratio; (c) under 20% damping ratio.

The 11 ground motions in the record set are shown in light colors, while the average of this data set is shown in dark colors. Figure 10(a) displays the input energy of ground motions at a 2% damping ratio; Figure 10(b) shows the input energy at a 5% damping ratio; and Figure 10(c) shows the input energy at a 20% damping ratio, including its average.

5. RESULTS AND DISCUSSION

This study examines changes across four earthquake record sets containing FD and NFD ground motions in the ZC and ZD soil classes, with damping ratios of 2%, 5%, and 20%. Using the ground-motion record sets, average input energies for the four sets were calculated at different damping ratios. The ground motions in each record set were analyzed sequentially, and the input energies obtained from the records and from the set average were plotted.

Figure 11 presents the average input energies of the earthquake record sets examined for different soil classes, damping ratios, and FD and NFD ground motions. Accordingly, the average input energy curves are shown as follows: FD ground motions of the ZC soil class in Table 1 — blue; the NFD earthquake record set of the ZC soil class — red; the FD ground motions of the ZD soil class, whose earthquake characteristics are specified in Table 3 — yellow; and the NFD ground motions in the ZD soil class — pink. Figure 11(a) shows the average input energy of all earthquake record sets at a 2% damping ratio. Figure 11(b) represents the change in ground motions at a 5% damping ratio. Figure 11(c) shows the average input energy of ground motions at a 20% damping ratio.

In the figure, the input energy generated by a set of 11 earthquake records containing forward directivity effects in the ZC soil class under different damping ratios, and the average input energy of this set, are shown. Accordingly, the average input energy peak of the FD earthquake records in the ZC soil class is calculated as 2.21 m^2/s^2 at a 2% damping ratio, while the peak average input energy is 1.87 m^2/s^2 at a 5% damping ratio. This value decreases to 1.36 m^2/s^2 when the damping ratio is increased to 20%.

Figure 11 presents the results of the analysis of the NFD 11 earthquake record for the ZC soil class. At a 2% damping ratio, the peak value of the average input energy is 1.56; m^2/s^2 increasing the damping ratio to 5% reduces it to 1.24 m^2/s^2. Increasing the damping ratio to 20% results in a value of 1.01 m^2/s^2.

The same figure shows the change in input energy of the earthquake record set for the ZD class as the damping ratio varies. An increase in the damping ratio significantly affects the average input energy to the system. At 2% damping, the peak average input energy was 4.36 m^2/s^2. While increasing the damping ratio to 5% reduces this value to 3.74 m^2/s^2, at 20% damping, the value decreases further to 2.84 m^2/s^2.

The effect of varying damping ratios on the average input energy for the ZD soil class is shown in Figure 11. At a damping ratio of 2%, the minimum damping ratio, the peak average input energy was determined to be 1.56 m^2/s^2. Increasing the damping ratio to 5% reduced the peak average input energy to 1.24 m^2/s^2, while increasing it to 20% reduced it to 0.99 m^2/s^2.

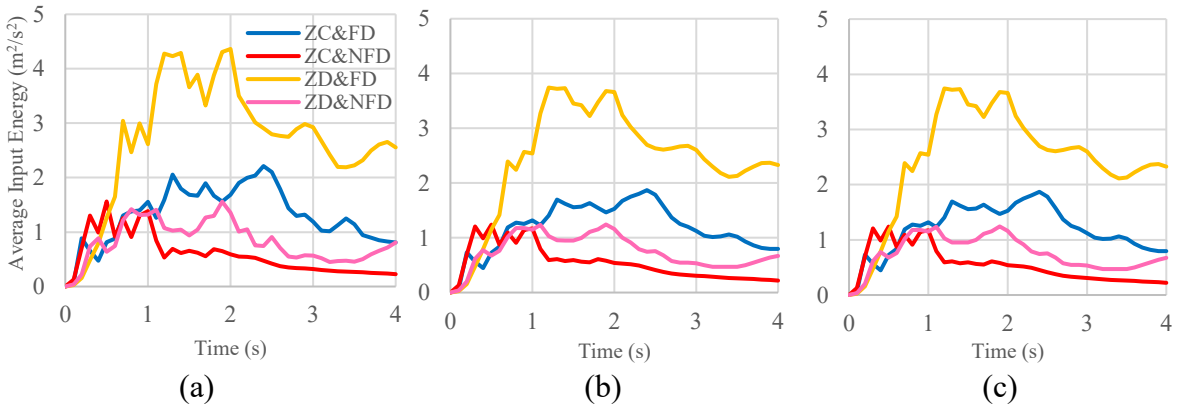


Figure 11. Average input energy of datasets (a) under 2% damping ratio; (b) under 5% damping ratio; (c) under 20% damping ratio.

Figure 11 shows that the average input energy for each soil class decreases significantly with increasing damping ratio. Increasing the damping ratio from 2% to 5% for FD ground motions in the ZC soil class reduces the average input energy by approximately 15.4%, whereas increasing it to 20% results in a 38% decrease. On the other hand, increasing the damping ratio from 2% to 20% for NFD ground motions in the ZC soil class decreases the peak average input energy by approximately 35%. Additionally, the rising damping ratio produces similar results for ground motions in the ZD soil class. Increasing the damping ratio from 2% to 20% for FD ground motions in the ZD soil class decreases the peak average input energy by 35%, while this decrease is approximately 36.5% for NFD ground motions in the ZD soil class.

For all damping ratios, FD ground motions in the ZD soil class have the highest peak values of average input energy. When forward directivity effects are considered, the average input energy for the ZD soil class is approximately twice that of the ZC soil class. On the other hand, when ground motions without forward directivity effects are compared, no significant difference is observed in the peak values of the average input energy between soil classes.

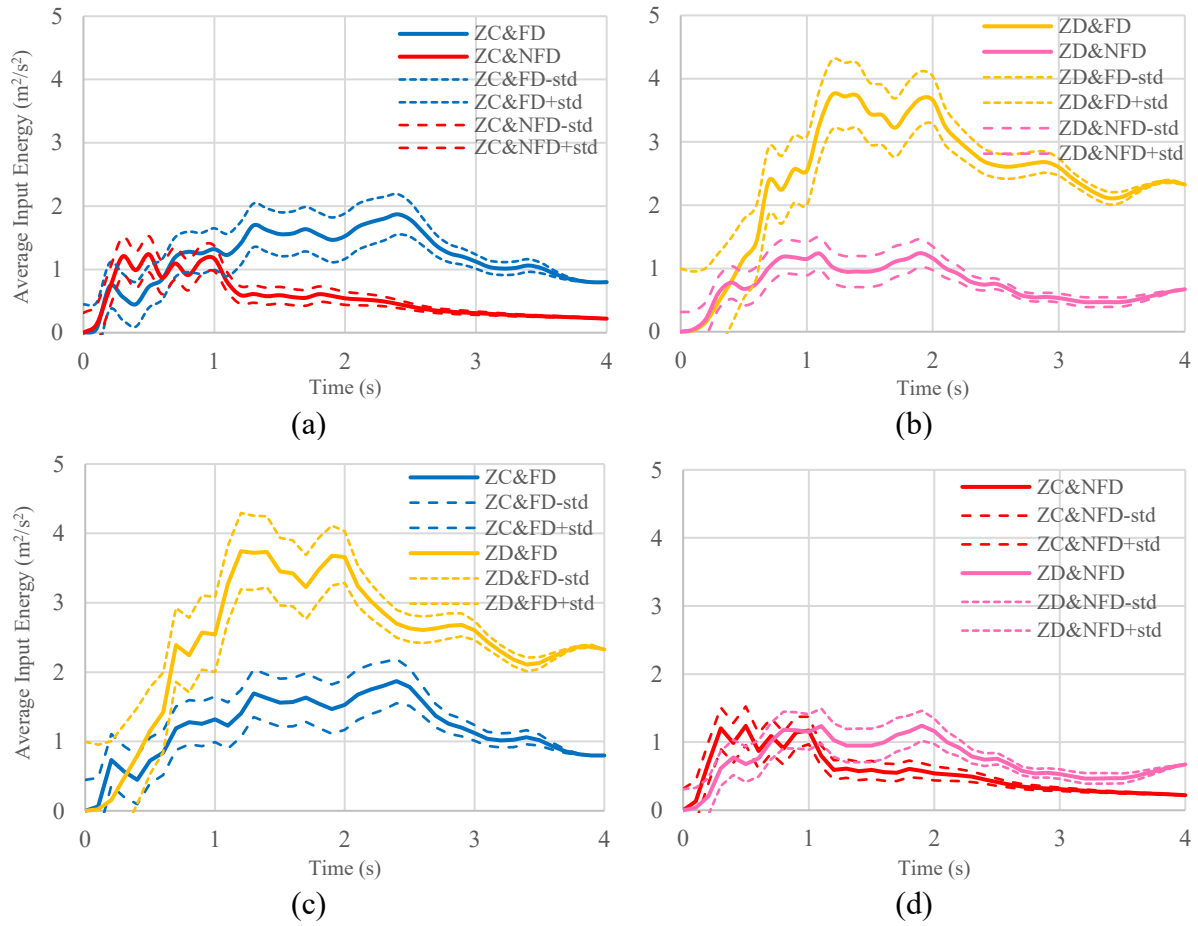


Figure 12. Average input energy of data sets under 5% damping ratio (a) under ZC soil class and FD effect; (b) under ZD soil class and FD effect; (c) under FD effect and different soil class; (d) under NFD effect and different soil class.

Figure 12 shows the graphs and their ± standard deviations, where the attenuation ratio was kept constant at 5%, to illustrate the effects of data obtained across different soil classes and forward directionality. The figure shows that earthquake record sets with higher average input energy have larger standard deviations and more scattered results. To illustrate this, Figures 12(a) and 12(b) show the variations in average input energy for the same soil class under different FD effects.

The presence of forward directivity effects is evident because these effects significantly alter the average input energy generated by ground motion within the same soil group. For example, when comparing the

peak values of average input energies at a 5% damping ratio in the ZC soil class, the peak value for FD ground motions is approximately 34% higher than that for NFD earthquake records. Similarly, in the ZD soil group, this ratio is approximately 67%.

On the other hand, Figures 12(c) and 12(d) reveal differences in the average input energy released when the soil class is changed, with the damping ratio and forward directivity held constant. Figure 12(c) shows the graphs obtained using FD ground motions for the ZC and ZD soil classes. Accordingly, the peak value of the average input energy released in the ZC soil class is half that in the ZD soil class. NFD ground motions in different soil classes are shown in Figure 12(d). The resulting graph shows that the peak values of the average input energies for the two soil classes are nearly equal. However, when this situation is examined over time, it is observed that the ZD soil class generally has higher average input energy. As a result of the weakening of the soil class, the average input energy imparted by ground motions is calculated to be higher.

The relationship between soil conditions and energy demand can be interpreted through the energy balance framework adopted in this study. The seismic input energy is governed by the interaction between ground acceleration and structural velocity. Softer soils, characterized by lower shear wave velocities, tend to amplify long-period ground motion components, leading to increased structural velocities and, consequently, higher input energy.

The forward directivity effect of ground motion increases the average input energy in both soil classes. This trend becomes more apparent when evaluating soil classes individually. For example, in the ZD soil class, this increase is particularly significant. Specifically, when all damping ratios are considered, the peak values of the average input energy of the FD and NFD ground motions in the ZD soil class differ by approximately 2.8-fold. In contrast, for the ZC soil class, increasing the damping ratio from 2% to 20% results in differences of approximately 35% to 51% between the FD and NFD ground motions.

The observed differences in average input energy demand between the ZC and ZD soil classes can be primarily attributed to site effects associated with V_{S30} and soil-dependent spectral amplification. Softer soils, such as ZD, are known to amplify long-period components of ground motions, resulting in increased velocity and displacement demands and, consequently, higher seismic input energy [17,27]. In addition, forward-directivity ground motions interacting with soft soil conditions tend to exhibit elongated pulse periods and sustained velocity pulses, which further enhance energy transfer to the structure [32,34]. Therefore, the higher input energy demands observed for the ZD soil class, particularly under forward-directivity effects, are not solely due to soil softness but also to the combined influence of site amplification and pulse–soil interaction characteristics of the selected ground motion records. Physically, the greater energy demand observed in soft soils subjected to forward-directivity motions results from the interaction between the pulse characteristics of near-fault ground motions and soil-controlled amplification mechanisms. Softer soils, characterized by lower shear-wave velocities and lower seismic impedance, tend to amplify long-period components of ground motion and allow more efficient transmission of seismic energy to the structure. When pulse-like motions associated with forward directivity interact with such soil conditions, the velocity pulse may become elongated, and its energy content may be further amplified by site effects. As a result, a larger proportion of seismic energy is transferred to the structural system within a short time interval. This combined pulse–soil interaction mechanism provides a physical explanation for the significantly higher input energy demands observed in the ZD soil class than those in the ZC soil class in the present study.

The higher input energy demands observed under forward-directivity ground motions, particularly for the ZD soil class, can be partly attributed to the concentration of seismic energy in pulse-like motions whose characteristic periods may interact with the structural period, as reported by Somerville et al. (1997) and Baker (2007) [32,34].

Although higher-mode effects were not explicitly considered in the present study, previous research has shown that seismic input energy in multi-degree-of-freedom systems is predominantly governed by the fundamental mode, particularly for pulse-like near-fault ground motions. Higher modes may contribute to localized force and acceleration demands; however, their contribution to total input energy is generally secondary compared to that of the first mode. Therefore, while the inclusion of higher modes

could modify the distribution of energy among structural components, the overall trends observed with respect to soil class, damping ratio, and forward-directivity effects are expected to remain qualitatively unchanged.

The graphs in Figure 12 show that the input energies for the ZC soil class in the short-period region are higher than those for the ZD soil. As shown in Figure 4, the acceleration spectra of ZC are higher than those of ZD in the short-period region.

6. CONCLUSION

This study investigates how soil class, forward directivity, and damping ratio affect the average input energy. Four earthquake record sets, varying by the inclusion of forward directivity, were created for two soil groups of different classes. These ground motions were used to analyze a single-degree-of-freedom structure and to calculate the average input energy for various damping ratios. The following conclusions were drawn from analyses conducted using the selected variables and records:

- Among all scenarios, FD ground motions in the ZD soil class exhibited the highest average input energy. The lowest energy demands were observed for ground motions in the ZC soil class, which exhibited no forward directivity effects. Weakening the soil, especially when forward directivity effects are included, results in the highest average input energy.
- Increasing the damping ratio always reduces the peak value of the average input energy. For the examined earthquake records, increasing the damping ratio from 2% to 20% reduces the peak average input energy by about 35%-40%.
- When the selected ground-motion characteristic changes from the absence of forward directivity to its presence, the average input energy increases by approximately 35%-50% in the ZC soil class, whereas in the ZD soil class the increase is almost threefold.
- Changing the soil class affects the peak value of the average input energy. For FD ground motions, the difference between ZD and ZC soils is approximately 50%. For NFD ground motions, changing the ground class does not produce a significant difference.
- The results also indicate that the interaction between pulse-like ground motions and soil-controlled amplification mechanisms plays an important role in governing seismic input energy demand.

Based on a limited number of selected earthquake records, forward directivity effects significantly increase the energy demand in seismic design, especially for structures located on weak soils. To address this, energy-based design, which incorporates the analysis of direct earthquake records, can significantly improve existing methods. Therefore, it is recommended that future studies apply this approach to a wider range of earthquake record sets, more soil classes, multi-degree-of-freedom systems, non-rigid soil-structure interactions, and nonlinear behavior.

Acknowledgements

This research received no specific grant from any funding agency in the public, commercial, or not-for-profit sectors.

Conflict of Interest Statement

There is no conflict of interest between the authors.

Statement of Research and Publication Ethics

The study is complied with research and publication ethics.

Artificial Intelligence (AI) Contribution Statement

This manuscript was entirely written, edited, analyzed, and prepared without the assistance of any artificial intelligence (AI) tools. All content, including text, data analysis, and figures, was solely generated by the authors.

Contributions of the Authors

Conceptualization and methodology were performed by Serkan Engin and Hasan Sesli. Writing, review, and final editing were carried out by Serkan Engin. Analysis and initial drafting were conducted by Yusuf Turgut.

REFERENCES

[1] EN 1998-1, Eurocode 8: Design of structures for earthquake resistance – Part 1: General rules, seismic actions and rules for buildings. Brussels, Belgium: European Committee for Standardization, 2004.

[2] FEMA 440, Improvement of Nonlinear Static Seismic Analysis Procedures: Guidelines. Washington, DC, USA: Federal Emergency Management Agency, 2005.

[3] Republic of Turkey Ministry of Environment, Urbanization and Climate Change, Turkish Building Earthquake Code (TBEC 2018) [Online]. Available: https://www.resmigazete.gov.tr/eskiler/2018/03/20180318M1-2.htm

[4] M. J. Kowalsky, G. A. MacRae, and M. J. N. Priestley, "Displacement-Based Methodology for Seismic Design Applied to Single Degree of Freedom Reinforced Concrete Structures," Report No. SSRP-94/16. La Jolla, CA, USA: University of California, San Diego, 1994.

[5] Z. Celep, *Deprem Mühendisliğine Giriş ve Depreme Dayanıklı Yapı Tasarımı*, 2nd ed., İstanbul, Türkiye. Press Mar. 2022.

[6] A. A. Dindar, A. Bozer, H. Özkaynak, Z. Müderrisoğlu and A. Güllü, "Effect of Soil Condition on the Energy Distribution of Mid-Rise RC Buildings," in *Energy-Based Seismic Engineering*, Cham, Switzerland, vol. 692, pp. 266–273, Jun. 2025, doi: 10.1007/978-3-031-97129-7_21.

[7] F. Çalım, A. Güllü and E. Yüksel, "Predicting Displacement Demands in SDOF Systems Using Seismic Input Energy: A Machine Learning Approach," in *4th International Civil Engineering & Architecture Conference,* Trabzon, Türkiye*,* vol. 1, pp. 505-513, May. 2025, doi: 10.31462/icearc2025_ce_eqe_744

[8] Z. Müderrisoğlu, A.A. Dindar, A. Bozer, H. Özkaynak, A. Güllü, F. Çalım and S. Hasanoğlu, "A Quantitative Investigation on the Effects of Flexure-Dominated Reinforced Concrete Column Characteristics on the Dissipated Energy," *Turkish Journal of Civil Engineering,* vol. 35, no. 2, pp. 87-102, Mar. 2024, doi: 10.18400/tjce.1272125

[9] A. Güllü, E. Yüksel, C. Yalçın, A.A. Dindar, H. Özkaynak and O. Büyüköztürk, "An Improved Input Energy Spectrum Verified by the Shake Table Tests," *Earthquake Engineering & Structural Dynamics,* vol. 48, no. 1, pp. 27-45, Sep. 2018, doi: 10.1002/eqe.3121

[10] O. Merter and T. Uçar, "İdeal Göçme Mekanizması İçin Enerji Esaslı Yapı Taban Kesme Kuvvetinin Belirlenmesi," *Dicle Üniversitesi Mühendislik Fakültesi Mühendislik Dergisi*, vol. 3, no. 7, pp. 409–420, 2016.

[11] G. W. Housner, "Limit Design of Structures to Resist Earthquakes," in *Proc. 1st World Conference on Earthquake Engineering*, vol. 5, pp. 5–13, 1956.

[12] İ. Ö. Dedeoğlu and Y. Calayır, "Yapı Sistemine Giren Enerji Bakımından TBDY (2018) ve DBYBHY (2007) Üzerine Bir İnceleme," *Dicle Üniversitesi Mühendislik Fakültesi Mühendislik Dergisi*, Mar. 2021, doi: 10.24012/dumf.851068.

[13] C. Uang and V. V. Bertero, "Evaluation of Seismic Energy in Structures," *Earthquake Engineering & Structural Dynamics*, vol. 19, no. 1, pp. 77–90, Jan. 1990, doi: 10.1002/eqe.4290190108.

[14] A. Benavent-Climent, L. G. Pujades, and F. López-Almansa, "An Energy-Based Methodology for the Assessment of Seismic Demand," *Earthquake Engineering & Structural Dynamics*, vol. 33, no. 10, pp. 1123–1145, 2004, doi: 10.1002/eqe.429

[15] R. K. Goel, "Seismic Response of Asymmetric Systems: Energy-based Approach," *Journal of Structural Engineering*, vol. 123, no. 11, pp. 1444–1453, Nov. 1997, doi: 10.1061/(ASCE)0733-9445(1997)123:11(1444)

[16] M. Hosseini and M. A. Vaseghinia, "A New Insight to the Earthquake Input Energy and Its Variation with Building's Dynamical Characteristics," *Proceedings of the 14th World Conference on Earthquake Engineering*, Beijing, China, Oct. 2008.

[17] A. A. Dindar, C. Yalçın, E. Yüksel, H. Özkaynak, and O. Büyüköztürk, "Development of Earthquake Energy Demand Spectra," *Earthquake Spectra*, vol. 31, no. 3, pp. 1667–1689, Dec. 2012, doi: 10.1193/011212eqs010m.

[18] A. A. Dindar, C. Yalçın, E. Yüksel, H. Özkaynak, and O. Büyüköztürk, "Development of Earthquake Energy Demand Spectra," *Earthquake Spectra*, vol. 31, no. 3, pp. 1667–1689, Aug. 2015, doi: 10.1193/011212EQS010M

[19] C. Yalçın, A.A. Dindar, E. Yüksel, H. Özkaynak and O. Büyüköztürk "Seismic Design of RC Frame Structures Based on Energy-Balance Method," *Engineering Structures,* vol. 237, Jun. 2021, doi: 10.1016/j.engstruct.2021.112220

[20] B. Akbaş, J. Shen, and H. Hao, "Energy Approach in Performance-Based Seismic Design of Steel Moment Resisting Frames for Basic Safety Objective," *The Structural Design of Tall Buildings*, vol. 10, no. 3, pp. 193–217, Jul. 2001, doi: 10.1002/tal.172.

[21] P. Khashaee, "Distribution of Earthquake Input Energy in Structures," *National Institute of Standards and Technology (NIST)*, Jan. 2003. [Online]. Available: https://nvlpubs.nist.gov/nistpubs/Legacy/IR/nistir6903

[22] A. Güllü, E. Yuksel, C. Yalçın, and O. Büyüköztürk, "Damping Effect on Seismic Input Energy and Its Verification by Shake Table Tests," *Advances in Structural Engineering*, vol. 24, no. 12, pp. 2669–2683, Apr. 2021, doi: 10.1177/13694332211010584.

[23] M. Neaz Sheikh, H.-H. Tsang, S. Yaghmaei-Sabegh, and P. Anbazhagan, "Evaluation of Damping Modification Factors for Seismic Response Spectra," in *Australian Earthquake Engineering Society Conference,* Hobart*,* Tasmania, Nov. 2013.

[24] M. Çelebi, "Preliminary Study of Correlation of Natural Periods and Damping Percentages of Tall Buildings in Several Countries," in *11th U.S. National Conference on Earthquake Engineering,* Los Angeles, California, United States, Jun. 2018.

[25] C. Zhai, D. Ji, W. Wen, W. Lei, and L. Xie, "Constant Ductility Energy Factors for the Near-Fault Pulse-Like Ground Motions," *Journal of Earthquake Engineering*, vol. 21, no. 2, pp. 343–358, Apr. 2016, doi: 10.1080/13632469.2016.1157529.

[26] B. Akbaş, Ü.M. Tuğsal, and F.İ. Kara, "An Evaluation of Energy Response and Cumulative Plastic Rotation Demand in Steel Moment-Resisting Frames Through Dynamic/Static Pushover Analyses," *The Structural Design of Tall and Special Buildings*, vol. 18, no. 4, pp. 405–426, Jun. 2008, doi: 10.1002/tal.442.

[27] A. Okur and M.A. Erberik, "Adaptation of Energy Principles in Seismic Design of Turkish RC Frame Structures. Part I: Input Energy Spectrum," in *Proceedings of the 15th World Conference on Earthquake Engineering*, Lisbon, Portugal, Sept. 2012.

[28] A. Okur and M.A. Erberik, "Adaptation of Energy Principles in Seismic Design of Turkish RC Frame Structures. Part II: Distribution of Hysteretic Energy," in *Proceedings of the Second European Conference on Earthquake Engineering and Seismology*, Istanbul, Türkiye, Aug. 2014.

[29] H. Sucuoğlu and F.S. Alıcı, "Elastic and Inelastic Near Fault Input Energy Spectra," *Proceedings of the 7th International Conference on Computational Methods in Structural Dynamics and Earthquake Engineering (COMPDYN)*, vol. 2, pp. 2196–2211, Jan. 2019, doi: 10.7712/120119.7070.18377.

[30] H. Zhang, Y.-G. Zhao, F.-W. Ge, Y. Fang, and T. Ochiai, "Estimation of Input Energy Spectrum from Pseudo-Velocity Response Spectrum Incorporating the Influences of Magnitude, Distance, and Site Conditions," *Engineering Structures*, vol. 274, Oct. 2022, doi: 10.1016/j.engstruct.2022.115165.

[31] S. Hasanoğlu, A. Güllü, A. A. Dindar, Z. Müderrisoğlu, H. Özkaynak, and A. Bozer, "Optimal Selection and Scaling of Ground Motion Records Compatible with Input Energy and Acceleration Spectra," *Earthquake Engineering & Structural Dynamics*, vol. 53, no. 7, pp. 2382–2404, Mar. 2024, doi: 10.1002/eqe.4114.

[32] P. Somerville, N. Smith, S. Punyamurthula and J. Sun, "Development of Ground Motion Time Histories for Phase 2 of the FEMA/SAC Steel Project," Sacramento, USA, Jan. 1997.

[33] T. Uçar and O. Merter, "Ductility demands for stiffness-degrading SDOF systems under pulse-like ground motions of the 2023 Pazarcık (Kahramanmaraş) earthquake," *Bullet of Earthquake Engineering*, vol. 22, no. 6, pp. 3243-3260, Mar. 2024, doi: 10.1007/s10518-024-01882-4.

[34] J.W. Baker, "Quantitative Classification of Near-Fault Ground Motions Using Wavelet Analysis," *Bulletin of the Seismological Society of America,* vol. 97, no. 5, pp. 1486-1501, Oct. 2007, doi: 10.1785/0120060255

[35] A. Bigdeli, H. Akbari, M. Alembagheri, H. Haghgou, and M. Matinfar, "Influence of Near-Field Ground Motions and Their Equivalent Pulses on Nonlinear Seismic Response of Intake-Outlet Towers and Predicting Based on Artificial Neural Networks," *Structures*, vol. 52, pp. 1051–1070, Apr. 2023, doi: 10.1016/j.istruc.2023.04.019.

[36] C.M. Uang and V.V. Bertero, "Evaluation of Seismic Energy in Structures," *Earthquake Engineering and Structural Dynamics,* vol. 19, no. 1, pp. 77-90, Jan. 1990, doi: 10.1002/eqe.4290190108

[37] E. Şafak, "Local Site Effects and Dynamic Soil Behavior," *Soil Dynamics and Earthquake Engineering,* vol. 21, no. 5, pp. 453-458, Jul. 2001, doi: 10.1016/j.istruc.2023.04.019

[38] A.K. Chopra, *Dynamics of Structures: Theory and Applications to Earthquake Engineering*, 3rd ed., Upper Saddle River, NJ, USA. Press 1995.

[39] MathWorks, MATLAB R2024b, Natick, MA, USA: The MathWorks, Inc., 2024.

[40] T. D. Ancheta, R. B. Darragh, J. P. Stewart, E. Seyhan, W. J. Silva, B. S. J. Chiou, K. E. Wooddell, R. W. Graves, A. R. Kottke, D. M. Boore, T. Kishida, and J. L. Donahue, PEER NGA-West2 Database, PEER Report No. 2013/03, Pacific Earthquake Engineering Research Center, University of California, Berkeley, 2013. [Online]. Available: https://ngawest2.berkeley.edu/

[41] SeismoSelect (2025), Seismosoft Earthquake Engineering Software Solutions.